Science Advances
AAAS

Manuscript Template

FRONT MATTER

Title

Tropical impacts of the Southern Ocean underestimated by mean-state biases.

Authors

Yue Dong,[1]* Kezhou Lu,[1] Yen-Ting Hwang,[2] Ruei-Jia Hu,[2] Paulo Ceppi,[3] Philipp Breul,[3,4] Lettie A. Roach[5], Clara Deser[6]

* To whom correspondence should be addressed. Email: ydong@atmos.ucla.edu

Affiliations

[1]Department of Atmospheric and Oceanic Sciences, University of California Los Angeles, USA.

[2]Department of Atmospheric Sciences, National Taiwan University, Taiwan.

[3]Department of Physics, Imperial College London, UK.

[4]Department of Geophysics and Meteorology, University of Cologne, Germany

[5]Alfred Wegener Institute, Helmholtz Centre for Polar and Marine Research, Germany.

[6]Climate and Global Dynamics Division, National Center for Atmospheric Research, USA.

Abstract

Observed sea-surface temperature (SST) trends over recent decades feature cooling in the tropical eastern Pacific and the Southern Ocean (SO). Growing evidence suggests that tropical cooling may partly stem from remote impacts of the SO. Using a hierarchy of multi-model simulations, we demonstrate that these teleconnections are robustly modulated by the mean-state inter-tropical convergence zone (ITCZ): models with a more realistic ITCZ simulate a stronger tropical SST response to SO forcing via stronger wind-evaporation-SST feedback. When realistic Antarctic meltwater forcing is included, correcting a model's tropical mean-state bias yields a stronger tropical cooling response to meltwater-driven SO cooling, improving the agreement between simulated and observed SST trends. Our results suggest that the SO's contribution to tropical warming patterns is systematically underestimated due to model mean-state biases. Improving representations of the mean-state climate is therefore critical for accurately assessing large-scale climate responses associated with historical and future warming patterns.

Teaser

The Southern Ocean's role in observed tropical cooling trends is systematically underestimated due to model mean-state biases.

MAIN TEXT

Introduction

Observations over recent decades have exhibited a distinctive sea-surface temperature (SST) trend pattern, characterized by broad cooling in the tropical eastern Pacific and the

Southern Ocean (SO) (*1*, *2*). This observed SST trend pattern has been linked to a wide range of changes in climate and extreme events across regional to global scales (*3–6*). However, reproducing this pattern remains a challenge for Global Climate Models (GCMs) participating in the Climate Model Intercomparison Project Phase 5 (CMIP5) and Phase 6 (CMIP6) (*1*, *2*, *7*), calling into question the credibility of GCM-based future climate projections in these regions.

A diverse pool of mechanisms has been put forward to explain the observed tropical SST trend pattern and model-observational discrepancies (*2*, *8*); however, consensus has yet to be reached on their relative importance. Tropical eastern Pacific cooling may arise from the transient oceanic response to greenhouse gas (GHG) forcing via the ocean thermostat mechanism (*9*, *10*), which indicates a possible persistence of the recent La Niña-like warming pattern into the near future under continued GHG forcing. On the other hand, contributions of anthropogenic aerosol emissions (*11*) and natural variability in the Pacific (*12*, *13*) may point to a possible shift toward an opposite El Niño-like warming pattern in the future. Unraveling the causes of the recent historical SST pattern is therefore critical for accurately predicting its future evolution.

Among the proposed mechanisms, remote impacts from the SO have received increasing attention. Like the tropical eastern Pacific, the SO has experienced substantial SST cooling over recent decades, particularly in the eastern Pacific sector (*1*, *14*). Various modeling evidence has revealed that SO cooling can drive a tropical La Niña-like SST response through atmospheric and oceanic teleconnections (*14–18*), suggesting a potential extratropical origin of the observed tropical cooling trends. The teleconnections can be initiated by surface temperature anomalies advected by the climatological mean winds (*14*) and are subsequently enhanced by positive feedbacks associated with the wind-evaporation-SST (WES) feedback (*19*), subtropical low-cloud feedback (*17*), and adjustments in ocean subtropical-tropical cells (*20*). Building on the proposed theories, recent studies demonstrated that a La Niña-like tropical SST pattern can arise from Antarctic ice-sheet meltwater input (*21*) and Antarctic ozone depletion (*22*, *23*), both of which are leading hypotheses for the observed SO cooling (*24–27*). Furthermore, directly nudging the observed SO SST anomalies in a fully-coupled GCM improved the agreement between simulated and observed tropical SST patterns (*18*), highlighting the SO's role as a pacemaker of tropical and global climate change (*28*).

However, several gaps remain in our understanding of the SO's contribution to the recent and near-future tropical warming patterns. First, although a La Niña-like tropical SST response to SO cooling is consistently simulated, models often use idealized SO forcings that are unrealistically strong (*29*), or simulate a tropical SST response that is weaker than observed (*21*). Second, existing modeling work exhibits varying degrees of tropical SST response (*17*, *18*, *30*), reflecting a wide spread in the strength of SO teleconnections. Furthermore, while the Southern Hemisphere (SH) subtropical eastern Pacific SST response is relatively robust, large uncertainty exists in the *equatorial* SST response (*21*, *31*), which governs remote impacts on the northern hemisphere (NH) hydroclimate (*32*, *33*) and global warming rate (*34*). Ultimately, despite progress from numerical model experiments, we are left with the question: to what extent has the SO contributed to the recent tropical SST trends and global climate change observed in nature?

In this study, we aim to better constrain SO teleconnection strength by examining the key physical processes that modulate SO teleconnections in individual GCMs and their inter-

model spread. We focus specifically on two factors: subtropical cloud feedback and the tropical mean-state climate. While the importance of subtropical cloud feedback has been widely recognized (*17*), the influence of the tropical mean-state in shaping the tropical response to SO forcing remains poorly understood. Like cloud feedbacks, tropical mean-state biases are prevalent in GCMs, most notably associated with the Intertropical Convergence Zone (ITCZ) known as the "double-ITCZ" problem (Fig. S1) (*35*, *36*). Although such mean-state biases may directly affect the local SST response to CO_2 forcing (*9*, *37*), here we focus on the tropical SST response to *remote* SO forcings. Specifically, we ask: do tropical mean-state biases affect the simulated strength of SO-tropical Pacific teleconnections? If so, what are the implications for understanding the observed tropical warming pattern?

To address these questions, we leverage multiple lines of evidence, including a suite of idealized simulations with the Community Earth System Model version 1 (CESM1, a CMIP5-class GCM), two multi-model intercomparison projects that uniquely incorporate SO thermal and freshwater forcings, and ensembles of transient historical simulations with realistic SO corrections using the NASA Goddard Institute for Space Studies version E2.1 climate model (GISS-E2-1-G, a CMIP6-class GCM). By comparing model results with observations, we provide new constraints on the remote tropical impact of SO SST changes.

Results

Sensitivity of the SO-tropical Pacific teleconnection strength

We begin by presenting results from idealized simulations with the slab-ocean configuration of CESM1 (Methods) that isolate the impacts of subtropical cloud feedbacks and the tropical mean state. Three control simulations are conducted, featuring distinct mean-state climates: (1) a "base" mean state, derived from a long control simulation of the fully-coupled CESM1, which carries all intrinsic model biases; (2) a "flux-adjusted" mean state, in which we modify climatological surface heat fluxes ("qflux") to better align the simulated SST and precipitation patterns with observations; (3) a "cloud-adjusted" mean state, in which we modify the model's radiation code to increase low-cloud-SST sensitivity to better match satellite observations. The modification is restricted to the SH subtropical eastern Pacific stratocumulus deck (contoured regions in Fig. S2F), where the model exhibits substantial biases in low cloud-SST sensitivity relative to satellite observations (*38*), and where local cloud feedback is central for regulating SO-tropics teleconnections (*17*). For each mean state, we perform a corresponding SO cooling experiment by imposing a constant qflux anomaly in the SO to induce local SST cooling.

First, we show the mean-state differences across the three control runs. Focusing on the tropical zonal-mean precipitation (Fig. 1C), the "base" control run exhibits a typical "double-ITCZ" bias, similar to other CMIP6 models. The "cloud-adjusted" control run produces a nearly identical precipitation pattern, retaining the same double-ITCZ bias. On the other hand, the "flux-adjusted" control run substantially improves the ITCZ representation, producing a more asymmetric precipitation pattern that closely matches observations (Fig. 1C and Fig. S3). This is because the "flux adjustment" effectively changes the mean-state SST distribution (Fig. S2A) and therefore precipitation patterns (Fig. S2B). By contrast, the "cloud adjustment" is designed to increase the sensitivity of low cloud amount to instantaneous SST *anomalies* relative to the mean state. Although

this modification results in an increased SST variance locally in the tropical eastern Pacific (*38*), it does not affect the SST mean state averaged over a long period (Fig. S2D; see also ref (*38*) for similar results using fully-coupled CESM1). Meanwhile, the shortwave (SW) cloud-SST feedback over the SH subtropical eastern Pacific region substantially strengthens in the "cloud-adjusted" control run (Fig. S2F), while remaining largely unchanged in the "flux-adjusted" control run (Fig. S2C). Overall, the "flux-adjustment" reduces the double-ITCZ bias, and the "cloud adjustment" strengthens subtropical cloud-SST feedback—both aligning better with observations.

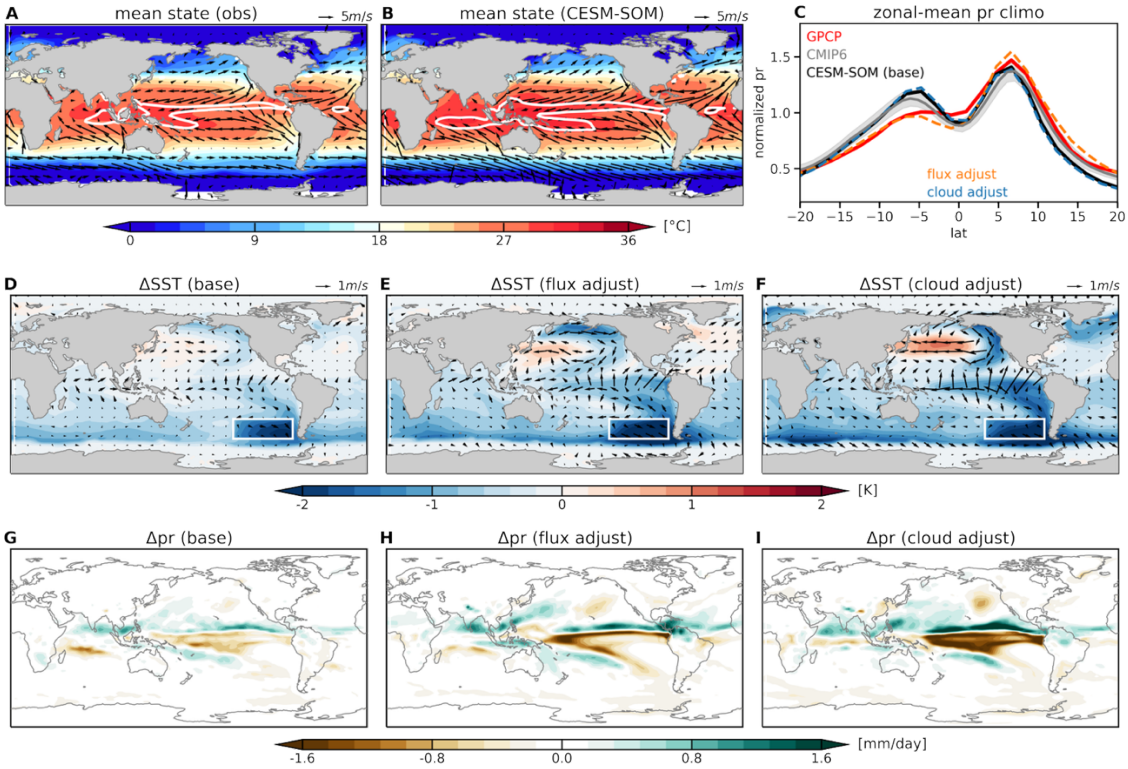

Figure 1: Mean-state climate and simulated response to Southern Ocean qflux perturbation in CESM1. *(**A, B**) Annual-mean climatology of SST (shading), surface winds (arrows), and precipitation (white contour denotes 6.5 mm/day level) in (A) observations and (B) CESM1 "base" control run. (**C**) Zonal-mean annual-mean precipitation normalized by the tropical mean from GPCP observations (red), CMIP6 multi-model mean (grey), CESM1 "base" control run (black), "flux-adjusted" control run (orange) and "cloud adjusted" control run (blue). The grey shading denotes one standard deviation across CMIP6 models. (**D–F**) Simulated annual-mean SST (shading) and surface wind (arrows) response to the imposed qflux perturbation in the "base", "flux-adjusted", "cloud-adjusted" simulations, respectively. White box illustrates where the anomalous qflux forcing is imposed (Methods). (**G-I**) Simulated annual-mean precipitation response.*

We next examine the quasi-equilibrium tropical response to the imposed SO qflux forcing (over the white box in Fig. 1D–F; Methods). With the "base" mean state, the imposed SO cooling produces a remote tropical response (Fig. 1D), including a La Niña-like cooling, strengthened SH trade winds, and a northward displacement of the ITCZ. This response pattern resembles the previously identified SO teleconnection response (*14*, *15*, *29*), driven by a series of coupled processes: SO SST anomalies can be first advected into the tropics by mean winds in the southeast Pacific, initiating an anomalous zonal SST gradient; this SST gradient is further amplified by subtropical cloud feedback and the WES feedback in the tropical eastern Pacific (14, 17). These tropical responses strengthen further in the flux- and cloud-adjusted mean states, both of which produce stronger

tropical eastern Pacific SST cooling (Fig. 1E, F), enhanced tropical zonal SST gradients (Fig. S4A), and more pronounced precipitation anomalies (Fig. 1H, I, Fig. S4B). These results suggest that both subtropical cloud-SST feedback and the mean ITCZ structure are critical for the remote response to SO cooling, and that biases in either may lead to underestimation of the teleconnection. A key question therefore arises: although the two biases are corrected separately by design in our experiments, do they influence the tropical response through independent mechanisms?

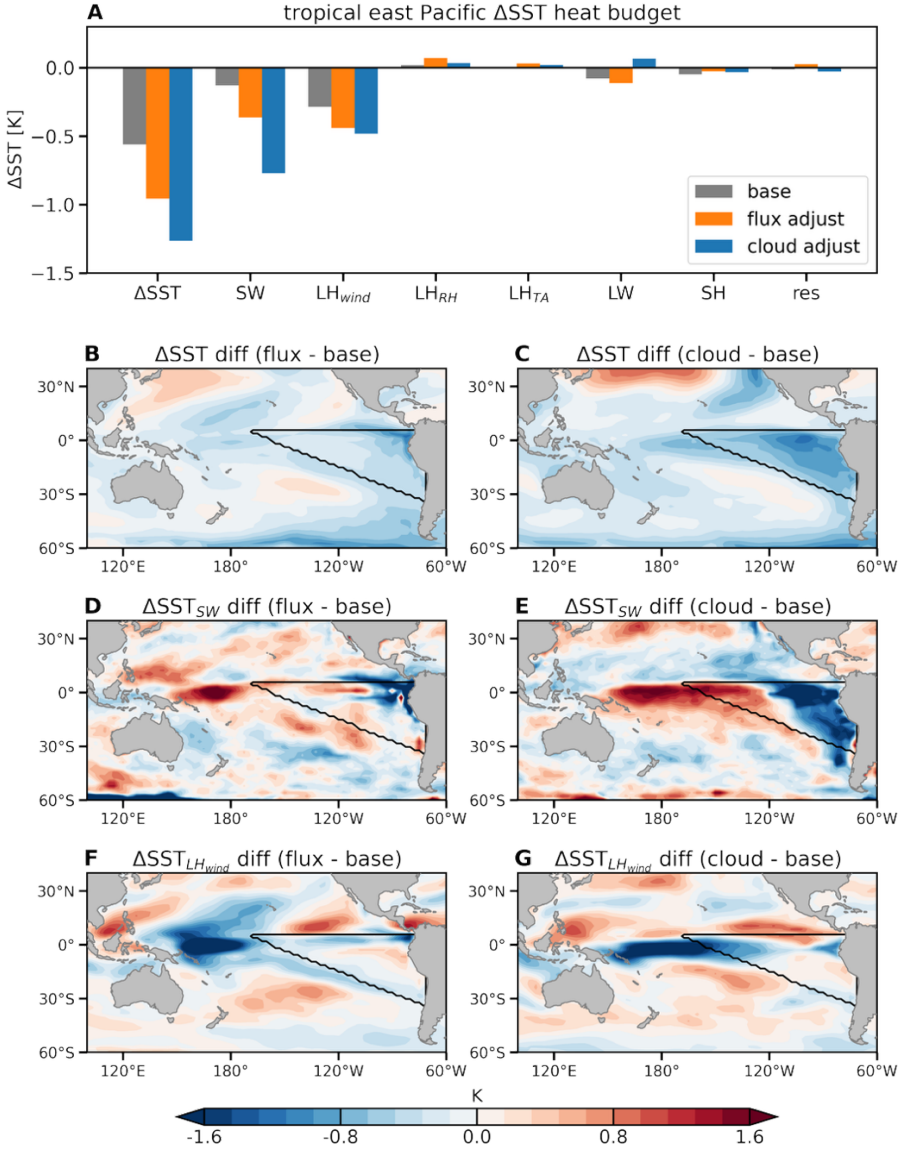

Figure 2: Surface energy budget analysis for the simulated tropical SST response in CESM1 simulations. *(A) Contributions of individual energy flux terms to the SST response averaged over the tropical eastern Pacific (the black triangular mask illustrated in panels B–G). From left to right are actual simulated SST response (ΔSST), contributions from shortwave flux (SW), latent heat flux due to wind speed changes (LH_{wind}), latent heat flux due to relative humidity changes (LH_{RH}), latent heat flux due to stability (LH_{TA}), longwave flux (LW), sensible heat flux (SH), residual (res). (**B–G**) Difference in the actual SST response (B, C), the SW-induced SST response (D, E), and the LH_{wind}-induced SST response (F, G) between "flux-adjusted" and "base" runs (left), and between "cloud-adjusted" and "base" runs (right).*

To understand the mechanisms, we perform a mixed-layer heat budget analysis of the tropical SST cooling response in all three simulations (Methods). Focusing on the broad

tropical eastern Pacific region (the triangular mask in Fig. 2B–G), we find that the SW radiative effect and the latent heat effect due to changes in wind speed (LH_{wind}) consistently dominate the SST response (Fig. 2A), confirming the leading roles of low cloud feedback and the WES feedback (*17*, *18*, *39*). However, their relative roles and spatial patterns differ across mean states. In the "cloud-adjusted" run, the tropical eastern Pacific SST cooling is predominately driven by SW flux (Fig. 2A), which accounts for most of the additional cooling relative to the "base" simulation (Fig. 2E). In contrast, the "flux-adjustment" produces stronger tropical cooling through an enhanced LH_{wind} effect over the broader trade wind region (Fig. 2F), with an additional contribution from the cloud SW effect that is mostly confined to the region off the coast of South America (Fig. 2D). This enhanced WES feedback is associated with the improved ITCZ mean state (Fig. S2A), characterized by stronger trade winds in the SH subtropical eastern Pacific and cross-equatorial southerlies converging into the band of deep convection north of the equator. These intensified mean-state winds enable stronger advection of SO SST anomalies into the tropical central Pacific and equatorial eastern Pacific, and also enhance the WES feedback, further amplifying the cooling.

Overall, the idealized CESM1 simulations suggest that, in addition to the subtropical cloud feedback, ITCZ representation is also critical to the strength of SO-tropical Pacific teleconnections. Importantly, the effect of an improved ITCZ is independent of improved cloud feedback in our model, implying an additional and previously underappreciated role for mean-state ITCZ modulation of SO teleconnections.

Inter-model spread in tropical response to SO SST forcing

Building on the mechanistic understanding of mean-state modulation derived from the single-model simulations, we next investigate if differences in mean-state biases further contribute to the inter-model spread in the simulated tropical SST response to SO cooling. Here, we analyze the Extratropical-Tropical Model Inter-comparison Project (ETIN-MIP) (*29*) experiments conducted within seven fully-coupled GCMs. In these simulations, solar flux is reduced between 65^{o}S and 45^{o}S to force the SH extratropical surface temperature to cool, which subsequently drives a La Niña-like response in the tropical Pacific (*16*, *17*, *29*). Although this tropical response is robust in the multi-model mean (Fig. 3D), its pattern and magnitude vary widely across individual models (Fig. S5).

Is the inter-model spread in the tropical SST response across ETIN-MIP connected to models' ITCZ biases? A first look at the precipitation mean state in ETIN-MIP's control simulations reveals diverse ITCZ structures across the models (Fig. 3A), but nearly all exhibit a consistent double-ITCZ bias. To quantify the bias, we define a precipitation asymmetry metric (pr^*) as the difference between NH and SH zonal-mean precipitation maxima, normalized by the tropical mean precipitation (Methods). Most models simulate a pr^* smaller than observed (Fig. 3B), reflecting the double-ITCZ bias. We then further regress the tropical eastern Pacific SST response (white box in Fig. 3D) to SH radiative cooling onto each model's mean-state pr^* across all seven models. A significant correlation ($p = 0.01$) is obtained (Fig. 3B), with pr^* explaining ~ 75% of the inter-model variance in the tropical eastern Pacific SST response. This indicates that models with a larger pr^* (i.e., smaller double-ITCZ bias) tend to simulate a stronger tropical eastern Pacific SST cooling response to SO forcing.

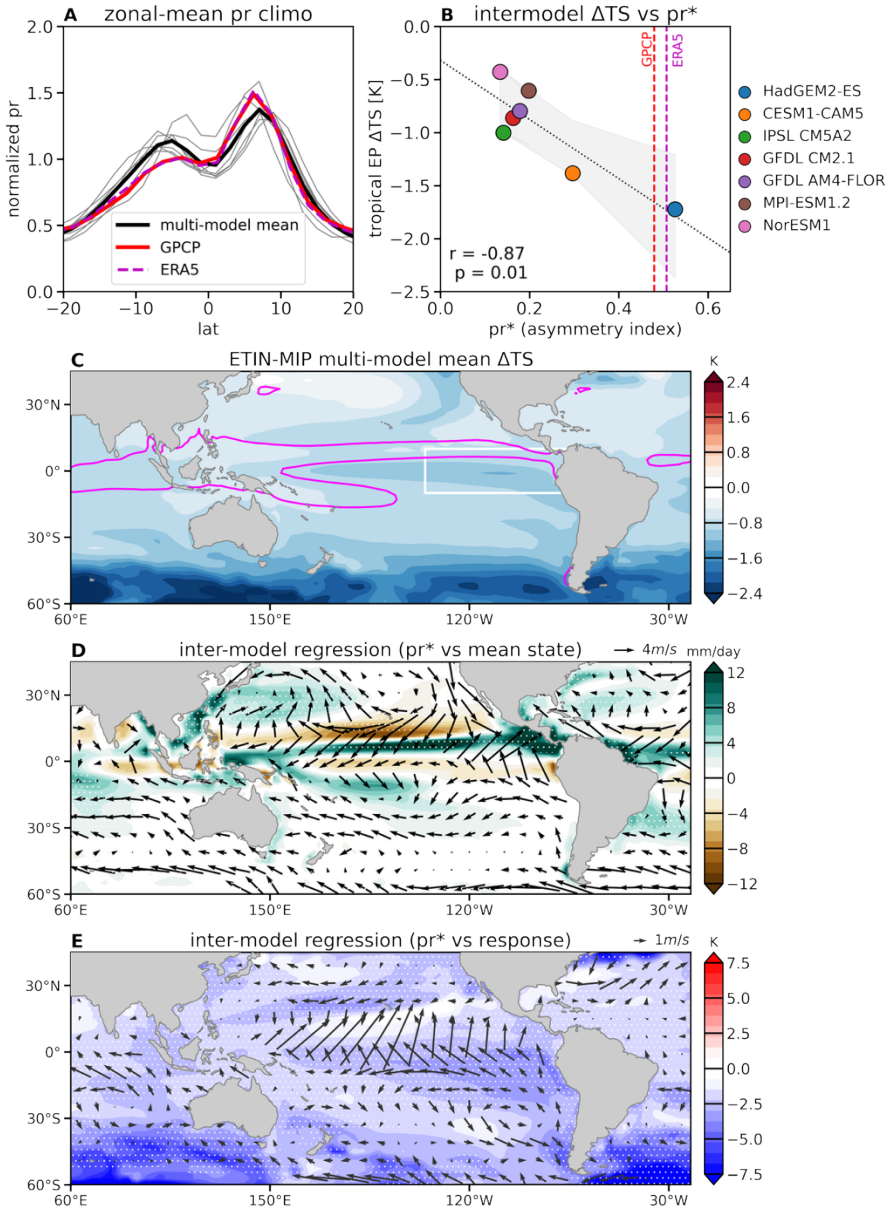

Figure 3: Mean-state climate and response to SO forcing in ETIN-MIP experiments. *(**A**) Annual-mean zonal-mean precipitation normalized by the tropical mean from observations and ETIN-MIP models. Solid red line denotes GPCP observations, dashed magenta line denotes ERA5; thick black line denotes the average of seven ETIN-MIP models, and thin grey lines denote individual models. (**B**) Inter-model correlation between tropical eastern Pacific SST response (the white box illustrated in panel D, spanning 10°S -10°N and 220°E – 290°E.) and mean-state pr*.The black dotted line denotes the linear regression across models (scatters); the grey shading represents the 95% confidence interval of the regression fit. The correlation coefficient (r) and p-value (p) are shown in the bottom left corner. (**C**) ETIN-MIP multi-model mean SST and surface wind response to SH extratropical forcing. Magenta contour denotes the 6 mm/day level of the annual-mean climatological precipitation. (**D**) Inter-model regression between mean-state precipitation and surface winds onto pr*. (**E**) Inter-model regression between local SST and surface wind response onto pr*. Stippling denotes where the inter-model regression is statistically significant at the 95% confidence level.*

The robust inter-model correlation between the *pr** index and the tropical eastern Pacific SST response (Fig. 3B) reflects a consistent modulation of the simulated SO teleconnection strength by the tropical mean state. Fig. 3D shows that models with a larger *pr** tend to simulate a mean-state climate with more precipitation to the north of the equator (and less to the south), as well as stronger surface southeasterly winds in the subtropical southeastern Pacific and more pronounced southerlies along the equator. Similar to the CESM1 "flux-adjusted" simulations, stronger mean winds can promote the

advection of SST anomalies from the SO to the tropical Pacific and enhance the WES feedback, thereby amplifying the SST cooling response in the trade wind regions (Fig. 3E).

While previous studies have found that a substantial portion of the inter-model spread in the tropical SST response to SO SST forcing is associated with differences in subtropical low-cloud feedbacks (*17*, *18*), here we demonstrate that differences in the mean-state ITCZ are another major source of the inter-model spread. There is no significant correlation between the mean-state *pr** index and the subtropical cloud feedback across GCMs (Fig. S6), suggesting that the two effects are largely independent. As all models share systematic double-ITCZ biases (Fig. 3B), accounting for these biases would imply a stronger SO-tropics teleconnection than currently simulated. Based on the ETIN-MIP models, we estimate that the tropical eastern Pacific SST response to SO forcing could be 70% stronger than the multi-model mean (with a 95% confidence interval of 20%–120%) if the models reproduced the observed ITCZ structure (Fig. 3B).

Constraining the tropical response to historical Antarctic meltwater

Idealized CESM1 simulations and ETIN-MIP experiments both suggest that SO-tropical Pacific teleconnections may be underestimated in current GCMs, reinforcing the possibility that the observed tropical eastern Pacific cooling trends may arise partly from the SO. While it remains unclear what causes the observed SO cooling trends and GCM warm biases, one increasingly recognized mechanism is Antarctic ice-sheet meltwater input—a process lacking in current GCMs. Accounting for Antarctic meltwater input in a variety of GCMs produces SO surface cooling and freshening response resembling observations (*24*, *25*, *40–42*). This is primarily because the meltwater-induced freshening increases upper-ocean stratification, reducing the upward heat transport from the relatively warm subsurface (*40*, *42*). A recent study (*21*) further showed that the meltwater-induced SO cooling can extend into the tropics, driving a tropical SST trend pattern closer to observations. Here we ask: Do model mean-state biases influence our estimates of the tropical response to Antarctic meltwater forcing? And if so, what are the implications for understanding historical warming patterns and model-observation discrepancies?

First, we leverage a recent multi-model project—the Southern Ocean Freshwater Input from Antarctica initiative (SOFIA) (*43*)— to examine the inter-model uncertainty in the tropical SST response to Antarctic meltwater forcing. SOFIA provides near-equilibrium meltwater hosing simulations with an idealized constant freshwater release around Antarctica (Methods). Preliminary results from eight fully-coupled GCMs show that the addition of freshwater yields a robust SO surface cooling response and Antarctic sea-ice expansion (*43*, *44*). We focus on the remote tropical impact and find that the multi-model mean near-surface air temperature (TS) response shows a La Niña-like tropical cooling pattern (Fig. 4C), consistent with the previous single model study (*21*). The magnitude of the tropical response, however, varies greatly across individual models (Fig. S7), along with a large spread in their precipitation mean state (Fig. 4A and Fig. S7).

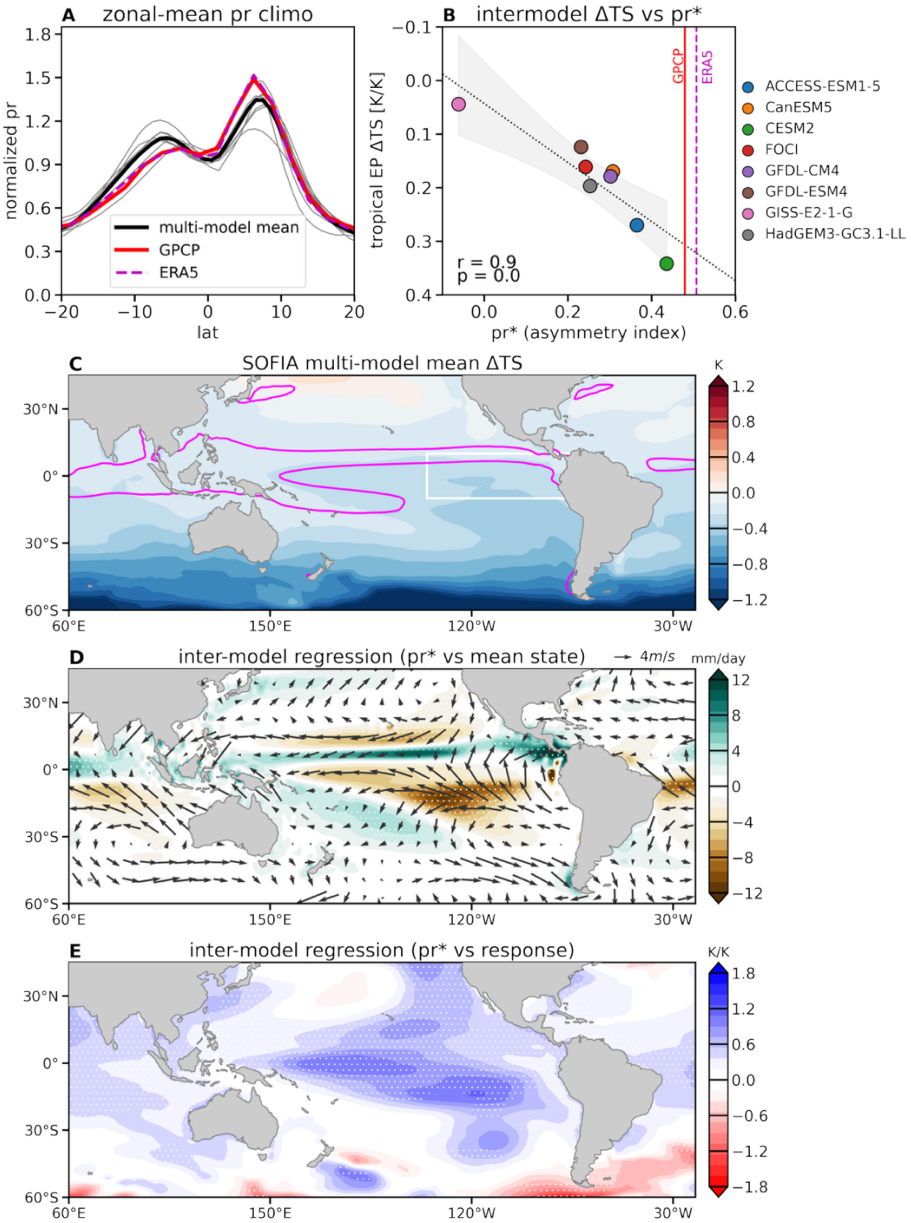

Figure 4: Mean-state climate and response to Antarctic meltwater in SOFIA meltwater experiments. *(**A**) Annual-mean zonal-mean precipitation normalized by the tropical mean from observations and SOFIA models. Similar to Fig. 3A, except thick black line denotes the average of seven SOFIA models, and the thin grey lines denote individual models. (**B**) Inter-model correlation between tropical eastern Pacific TS response and mean-state pr*. The tropical TS response is normalized by each model's SO (south of 60°S) TS response and is averaged over 10°S -10°N and 220°E – 290°E. The black dotted line denotes the linear regression across models (scatters); the grey shading represents the 95% confidence interval of the regression fit. The correlation coefficient (r) and p-value (p) are shown in the bottom left corner. (**C**) Multi-model mean TS and surface wind response to Antarctic meltwater input. Magenta contour denotes the 6 mm/day level of the annual-mean climatological precipitation. (**D**) Inter-model regression between mean-state precipitation and surface winds onto pr*. (**E**) Inter-model regression between normalized TS and surface wind response onto pr*. Stippling denotes where the inter-model regression of normalized TS is statistically significant at the 95% confidence level.*

To quantify the spread in tropical TS response related to the mean-state ITCZ, we repeat the regression analysis with *pr**. As the SO local TS cooling response to meltwater input is highly model-dependent, which we expect is not directly driven by tropical processes, we normalize the tropical TS response for each model by its SO TS change before performing

the regression analysis. The results show that mean-state pr^* inter-model differences again explain a major portion (~80%) of the inter-model spread in the normalized tropical TS response (Fig. 4B). Models with a greater mean-state pr^* have a reduced precipitation bias in the SH tropics and therefore stronger mean-state trade winds and cross-equatorial meridional winds in the tropical eastern Pacific (Fig. 4D). These intensified mean-state winds in turn drive a stronger tropical TS response to meltwater-driven SO cooling (Fig. 4B and 4E). We note that the regression maps of precipitation climatology and TS response from the ETIN-MIP and SOFIA models are broadly similar but exhibit notable spatial differences (c.f. Fig. 3 and Fig. 4). The differences in precipitation climatology (Fig. 3D vs Fig. 4D) likely arise from differences in the model ensembles and the lengths of their control simulations. For the differences in TS response patterns (Fig. 3E vs Fig. 4E), in addition to model dependence, an important factor is the distinct forcing applied in each experiment. The ETIN-MIP experiment imposes a constant top-of-atmosphere radiative forcing that cools the SO surface radiatively, whereas the SOFIA experiment imposes a freshwater forcing that induces SO cooling via ocean dynamic feedback while conserving the global energy balance. As a result, the temporal and spatial scales of the SO temperature response and the associated tropical response are expected to differ between the two ensembles.

The SOFIA meltwater simulations confirm that the systematic double-ITCZ mean-state biases in current GCMs lead to an underestimation of the tropical TS response to Antarctic meltwater input. This implies that the contribution of historical Antarctic meltwater to observed tropical SST trends may have been larger than currently simulated. To test this hypothesis and better constrain the tropical impact of historical Antarctic meltwater input, we analyze historical transient meltwater simulations developed with the NASA GISS-E2-1-G model (Methods). To our knowledge, this is the first ensemble of CMIP6 simulations that incorporates observationally constrained Antarctic meltwater input from 1990–2021(*25*, *45*). The imposed anomalous meltwater flux induces SO local SST cooling trends (*25*, *45*)(Fig. 5D), improving agreement with observations (*45*). Outside of the SO, however, the meltwater input exerts only a marginal influence on the tropics (Fig. 5E), producing insignificant differences in the simulated tropical eastern Pacific TS trends (Fig. 5B). This result seems to suggest a negligible contribution of Antarctic meltwater to the observed tropical warming pattern.

However, findings from our CESM1 idealized simulations suggest that model mean-state biases in subtropical cloud feedback and ITCZ may lead to a substantial underestimation of the SO teleconnection strength. In particular, GISS-E2-1-G exhibits a severe double-ITCZ bias (Fig. 5E) among the CMIP6 models (Fig. 4B). By adjusting its SO-tropics teleconnection strength based on inter-model pr^* correlations (Methods), we find that the tropical impacts of Antarctic meltwater input would have been more pronounced had the model reproduced the observed ITCZ mean state (Fig. 5F). Accounting for both the meltwater-induced SO changes and the observationally-constrained SO teleconnection strength brings the simulated tropical TS trends over the broad eastern Pacific trade wind regions into closer agreement with observations (Figs. 5B and 5D). This new constraint thus reveals a previously underestimated role of Antarctic meltwater input in the observed tropical La Niña-like cooling trends. While growing efforts are underway to develop interactive ice-sheet coupling, our results highlight that reducing persistent biases in the tropical mean state (e.g., the double ITCZ bias) remains equally critical for accurately capturing the large-scale impacts of meltwater input.

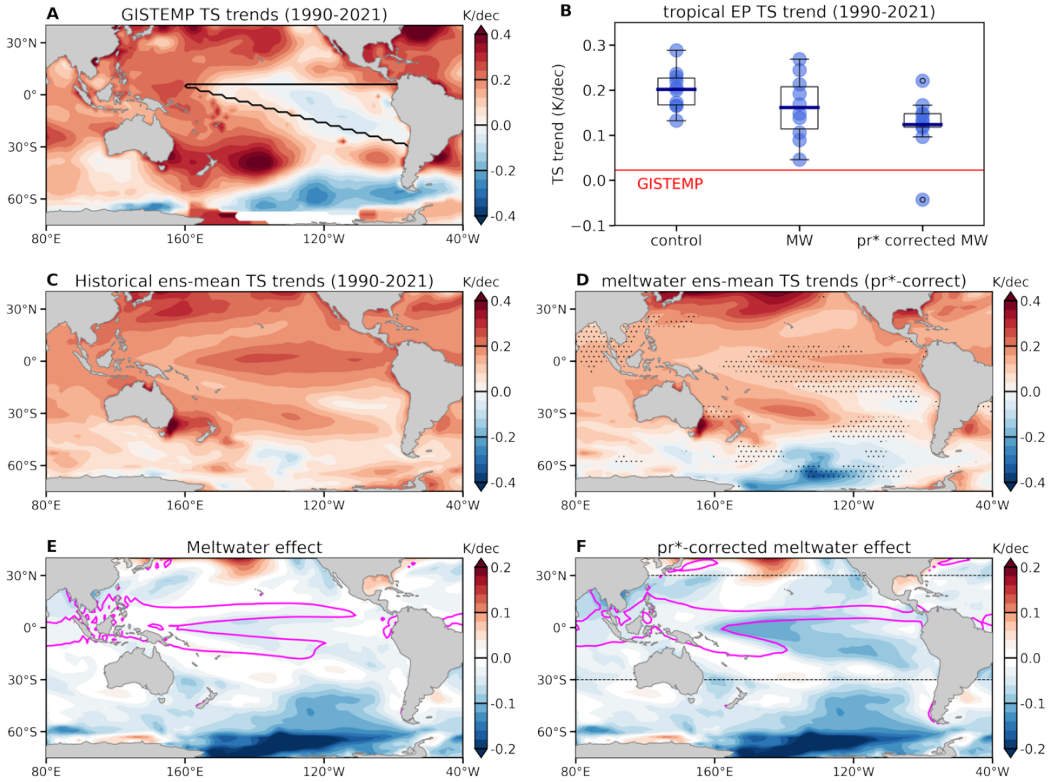

Figure 5: Observed and GISS-E2-1-G simulated TS trends over 1990–2021. *(**A**) TS trends from the GISTEMP v4 observational dataset. (**B**) Tropical eastern Pacific TS trends (averaged over the triangular region illustrated in panel A) in the historical control ensemble, historical meltwater ensemble, and adjusted values based on the pr* regression and observed pr* (Methods). Thick blue lines represent the mean of each ensemble. Note that the results of the control ensemble (left column) and the adjusted ensemble (right column) are statistically different from each other at the* 95% *confidence level. The triangular area is chosen to capture the most pronounced tropical Pacific cooling over this period. (**C**) TS trends from the ensemble-mean of GISS-E2-1-G historical control simulations. (D) TS trends from the ensemble-mean of GISS-E2-1-G meltwater simulations after applying the pr* correlation (panel C + panel F). Stippling represents grid points where the local difference between the control and corrected meltwater simulations is statistically significant at the 95% level. (**E**) TS trend difference between historical and meltwater simulations, representing the meltwater impact. Magenta contour denotes the 6 mm/day level of the annual-mean climatological precipitation from GISS-E2-1-G historical control simulations (1950–2021). (**F**) Similar to (E) except the tropical TS response (between 30ºS–30ºN, illustrated by grey lines) is adjusted based on the SOFIA inter-model pr* regression (Fig. 4), assuming that the GISS-E2-1-G model had reproduced the observed ITCZ. Magenta contour denotes the 6 mm/day level of the annual-mean climatological precipitation from ERA5 reanalysis (1950–2021).*

Discussion

Observed SST trends over recent decades feature unique cooling in the tropical eastern Pacific and the Southern Ocean. The La Niña-like tropical SST trend pattern has caused a broad range of extratropical changes via the well-established atmospheric teleconnection pathways (*46*, *47*), influencing SH midlatitude circulation (*48*), precipitation(*49*) , and Antarctic sea ice (*50*). However, how the SO influences the tropics and to what extent this SO-originated teleconnection contributes to the observed tropical SST pattern remains an area of active research. Using a hierarchy of model simulations with distinct SO thermal and freshwater forcings, we here demonstrate that the tropical mean-state climate, particularly the position and strength of the ITCZ, strongly modulates SO-tropical Pacific teleconnections. Models with a more realistic ITCZ tend to simulate stronger mean-state winds in the tropical eastern Pacific, which enable a stronger tropical SST response to SO forcing via mean-wind advection and the WES feedback. Given that GCMs commonly

struggle with the "double-ITCZ" bias, our results imply that the remote tropical impacts of the SO may have been systematically underestimated, and that model deficiencies in the tropics may have biased our understanding of the broader impacts of polar climate change.

These results underscore the importance of improving the model mean state for accurately simulating historical climate change. For example, when forced with observed SO SST anomalies, CESM1 and CESM2 produce markedly different tropical SST responses (*18*, *30*). The stronger tropical response in CESM2 has been attributed to its more realistic subtropical cloud feedback (18). However, CESM2 also has a reduced double ITCZ bias compared to CESM1 (Fig. S8), which may contribute to its improvement in tropical SST trends. Thus, improving *both* cloud feedbacks and the ITCZ mean state is essential for understanding large-scale teleconnections and developing the next generation of climate models.

More broadly, improving model representation of SO teleconnections could provide insights into tropical variability and predictability. Recent work has shown promising advances in tropical decadal prediction from improved simulations of the SO in a high-resolution GCM (*51*). A more realistic mean state would likely yield a stronger tropical SST response to SO changes, with potential implications for equatorial variability.

Despite recent cooling, the SO is projected to experience greater future warming than the global average under increased CO_2 forcing (*52–54*). Even in recent years (post–2016), rapid sea-ice loss and ocean subsurface warming around Antarctica have been observed, indicating a possible regime shift (*55*, *56*) in contrast to the cooling trends in earlier decades (*57*). Future SO warming is expected to exert broad remote influences, including effects on tropical warming patterns (*31*), NH midlatitude precipitation (*33*) and Arctic warming (*58*). Our study suggests that the tropical impacts of the observed SO changes, regulated by the tropical mean-state climate, may provide an insightful emergent constraint on future projections. Therefore, accurately assessing global climate responses to SO changes hinges not only on models faithfully representing polar processes under global warming (e.g., Antarctic ice sheet dynamics), but also on their ability to realistically simulate the mean-state climate. Advancing the representation and understanding of the remote climate impacts of the SO is thus critical for accurately constraining future global climate change.

Materials & Methods

CESM1 simulations. Simulations with mean-state modifications shown in Fig. 1 and Fig. 2 are carried out by a slab-ocean configuration of the Community Earth System Model version 1 (CESM1) with the Community Atmospheric Model version 4 (CAM4) at 2-degree horizontal resolution. All simulations are forced by a qflux climatology (e.g. prescribed ocean heat transport) and radiative forcing agents (greenhouse gases, aerosols, solar cycle, etc.) at the present-day climatological levels. The ocean mixed-layer depth is set to a uniform 50 m in all simulations to ensure consistency. We conduct three sets of simulations—"base", "cloud adjusted", and "flux adjusted"—each containing a control run and a SO-cooling experiment. For all three groups, the quasi-equilibrium responses are taken from the average of the last 30 years of the corresponding control and SO-cooling simulations.

For the "base" case, the control run is carried out for 120 years and uses a qflux climatology derived from a long piControl simulation within the fully-coupled CESM1. The corresponding SO-cooling experiment is branched from the 61st year of the control run and carried out for 60 years. Its qflux climatology is identical to that in the control run, except uniform negative qflux anomalies of 15W/m^2 are added over the southeast Pacific sector of the SO (55^{o}S–35^{o}S, 220^{o}E–280^{o}E), following the setup in (*14*).

For the "cloud adjusted" case, both the control and the SO-cooling simulations are branched from the 61st year of the "base" control simulation and carried out for another 60 years. In both control and SO-cooling simulations, we apply the cloud modification developed by ref (*38*) to the SH subtropical eastern Pacific stratocumulus deck (contoured regions in Fig. S2), a region where low cloud amount-SST sensitivity in CAM4 is significantly lower than that in the MODIS observations (*38*). The method is based on cloud-controlling factor analysis (*59*), which identifies the cloud sensitivity to a set of known physically important variables. Adjusting the sensitivity to these variables directly, rather than their impact through cloud formation processes, gives more control and better understanding over the adjustment. While the actual physical processes are circumvented, for this study, the relevant radiative impact is captured. Specifically, the cloud amount correction is set to be -3% of the local low-cloud amount anomaly per degree of local SST anomaly. The perturbation is then added to all cloud layers at or below 700 hPa at every radiation time step, proportional to the instantaneous SST anomaly relative to the SST mean state from the "base" control run. The modification is only applied in the CAM4 radiative transfer code to account for the radiative effect of enhanced low-cloud sensitivity. The qflux climatology data used in the control and SO-cooling simulations are identical to those used in the two "base" simulations.

The "flux adjusted" control and SO-cooling simulations are similar to the "base" simulations, except the control qflux climatology is derived from a long "flux-corrected" piControl simulation in CESM1-CAM4, where an annual-cycle of surface heat flux anomalies is applied to nudge the model's SST mean state to observations (*14*). The qflux anomalies over the SO are further added to this flux-adjusted qflux climatology for its SO-cooling simulation. The control run is conducted for 120 years and the SO-cooling simulation is conducted for 60 years, branched off from the 61st year of the control run.

Observations and CMIP6 models. We use precipitation observations from the Global Precipitation Climatology Project (GPCP) (*60*) and ERA5 Reanalysis (*61*). We also analyze 24 CMIP6 models and obtain the modeled precipitation climatology from their historical (1979–2014) and SSP3-7.0 (2015–2024) simulations, with one ensemble member per model. Both observed and modeled precipitation mean states are computed using annual means over 1979–2024. In Fig. 5, we use TS observations from GISTEMP v4 dataset (*62*) to compute the equatorial eastern Pacific TS trend over 1990–2021.

Surface energy budget analysis. We perform a mixed-layer heat budget analysis to decompose the contributions to the tropical SST response in CESM1 SO-cooling simulations. Following previous studies (*15*, *16*, *19*, *30*), we consider the surface energy budget as:

$$\rho C_p H \frac{\partial T'}{\partial t} = SW' + LW' + LH' + SH' + res \quad (1)$$

The left-hand side represents the mixed-layer heat storage, with ρ being the density of ocean, C_p the specific heat of the ocean, H the ocean mixed-layer depth and T surface temperature (i.e. SST over the ocean). The right-hand side represents the mixed-layer heat budget terms, with *SW* presenting surface shortwave flux, LW surface longwave flux, LH latent heat flux, SH sensible heat flux, and res residuals (all heat fluxes are defined as positive downward). The prime symbol $'$ represents the anomalies between the control and the SO-cooling simulations (the response). Since our CESM1 simulations are quasi-equilibrium, the left-hand side (the tendency term) is close to zero. Based on the linearized bulk formula for evaporation, latent heat changes associated with Newtonian cooling can be simplified as $\alpha\overline{LH}T'$where $\alpha \equiv \frac{L_v}{R_v T^2} \approx 0.06\ K^{-1}$, $\overline{LH}$ is the climatological mean LH. Eq. (1) can thus be rewritten into a diagnostic equation for the SST response:

$$T' = \frac{SW' + LW' + LH'_{wind} + LH'_{RH} + LH'_{TA} + SH' + res}{\alpha\overline{LH}} \quad (2)$$

where LH'_{wind}, LH'_{RH}, LH'_{TA} represent latent heat trend changes due to changes in wind speed, changes in relative humidity and changes in stability, respectively.

ITCZ index. The precipitation asymmetry index (pr^*, unitless) is defined as the difference between the NH (0–15°N) and SH (15°S–0) zonal-mean precipitation maxima, normalized by the tropical mean precipitation (15°S–15°N). Averaging precipitation over the Pacific (e.g., between 120°E–330°E) yields similar results.

SOFIA meltwater simulation. We use two experiments provided by the SOFIA project (*43*), *piControl* and *antwater* (in Tier 1), which are currently available for eight GCMs. The first is identical to the CMIP6 piControl setup, with no additional ice-sheet meltwater included. The second is the idealized meltwater hosing experiment, branched from the piControl simulation. It applies a freshwater flux anomaly of 0.1 Sv at the ocean surface around Antarctica. The antwater simulations are generally carried out for > 100 years, and we use the last 30 years to obtain quasi-equilibrium response. As the "*tos*" (sea-surface temperature) and "*ts*" (surface temperature) variables are not readily available for most of SOFIA models, we use "*tas*" (near-surface air temperature) instead for the analysis. For each model, we normalize the tropical TS response by its average over Antarctica (60°S–90°S, including both ocean and land), before conducting the inter-model regression analysis.

GISS-E2-1-G meltwater simulation and analysis. We present results from two ensembles of transient historical simulations conducted with the NASA Goddard Institute for Space Studies (GISS) version E2.1 climate model (GISS-E2-1-G). GISS-E2-1-G is a CMIP6-class fully-coupled global climate model, which exhibits relatively low biases in Southern Ocean SST trends compared to other models (*1*).

The first ensemble consists of 10 members of standard CMIP6 simulations spanning 1950–2021, denoted as "control" runs. From 1950–2014, the simulations used the CMIP6 "historical" forcing scenario with all time-varying radiative forcing agents; extensions from 2015–2021 used observed greenhouse gases and solar forcing while keeping other compositions and land use changes at 2014 levels. The second ensemble (*25*, *45*) also consists of 10 members and incorporates time-varying anomalous freshwater based on the observed post–1990 "ice imbalance" from Antarctica and Greenland ice sheets constrained by satellite observations (*63*). Note that because satellite altimetry-based

estimates of Antarctic ice imbalance are unavailable before 1990, this ensemble spans 1990–2021. Meltwater is added to the Southern Ocean (500 km wide around the Antarctic continent) uniformly from the surface to 200 m below. The same time-varying radiative forcings as in the control ensemble are used. To our knowledge, this historical meltwater ensemble within GISS-E2-1-G is the first set of CMIP6 simulations that implement observationally constrained Antarctic meltwater (*25*, *45*). The meltwater-induced surface temperature response is obtained by comparing the ensemble means of control and meltwater simulations.

We further correct the meltwater-induced tropical TS anomalies (between 30°S–30°N) based on the model's mean-state ITCZ. Specifically, we first compute the pr^* values from GISS-E2-1-G historical control simulations and ERA5 reanalysis over 1950–2021, denoted as pr^*_{ERA5} and pr^*_{GISS}, respectively. We then compute the adjusted tropical TS response ($\Delta TS^*_{tropics}$) as:

$$\Delta TS^*_{tropics}(x,y) = (pr^*_{ERA5} - pr^*_{GISS}) \frac{\partial\left(\frac{\Delta TS_{tropics}(x,y)}{\Delta TS_{SO}}\right)}{\partial pr^*} \Delta TS_{SO} + \Delta TS_{tropics}(x,y) \quad (3)$$

where $\frac{\partial\left(\frac{\Delta TS_{tropics}(x,y)}{\Delta TS_{SO}}\right)}{\partial pr^*}$ represents the coefficient from the inter-model regression of normalized TS response onto pr^*across eight SOFIA models (shown in Fig. 4E), ΔTS_{SO} is the TS response averaged over the SO (60°S–90°S), and $\Delta TS_{tropics}(x,y)$ is the originally simulated tropical TS response pattern. In our estimate, we retain ΔTS_{SO} from the meltwater simulations unchanged, and only apply the pr^*adjustment to the tropical TS response pattern. The adjusted tropical response $\Delta TS^*_{tropics}(x,y)$ thus represents the more realistic tropical response to the simulated meltwater-driven SO TS changes, assuming the model had accurately reproduced the observed ITCZ (pr^*).

References

1. R. C. Wills, Y. Dong, C. Proistosecu, K. C. Armour, D. S. Battisti, Systematic climate model biases in the large-scale patterns of recent sea-surface temperature and sea-level pressure change. *Geophys. Res. Lett.* **49**, e2022GL100011 (2022).

2. M. Watanabe, S. M. Kang, M. Collins, Y.-T. Hwang, S. McGregor, M. F. Stuecker, Possible shift in controls of the tropical Pacific surface warming pattern. *Nature* **630**, 315–324 (2024).

3. Y. Dong, K. C. Armour, C. Proistosescu, T. Andrews, D. S. Battisti, P. M. Forster, D. Paynter, C. J. Smith, H. Shiogama, Biased estimates of equilibrium climate sensitivity and transient climate response derived from historical CMIP6 simulations. *Geophys. Res. Lett.* **48**, e2021GL095778 (2021).

4. M. J. Alessi, M. A. Rugenstein, Surface temperature pattern scenarios suggest higher warming rates than current projections. *Geophys. Res. Lett.* **50**, e2023GL105795 (2023).

5. M. Zhao, T. Knutson, Crucial role of sea surface temperature warming patterns in near-term high-impact weather and climate projection. *Npj Clim. Atmospheric Sci.* **7**, 130 (2024).

6. K. C. Armour, C. Proistosescu, Y. Dong, L. C. Hahn, E. Blanchard-Wrigglesworth, A. G. Pauling, R. C. Jnglin Wills, T. Andrews, M. F. Stuecker, S. Po-Chedley, others, Sea-surface temperature pattern effects have slowed

global warming and biased warming-based constraints on climate sensitivity. *Proc. Natl. Acad. Sci.* **121**, e2312093121 (2024).

7. I. R. Simpson, T. A. Shaw, P. Ceppi, A. C. Clement, E. Fischer, K. M. Grise, A. G. Pendergrass, J. A. Screen, R. C. Wills, T. Woollings, others, Confronting Earth System Model trends with observations. *Sci. Adv.* **11**, eadt8035 (2025).

8. S. Lee, M. L'Heureux, A. T. Wittenberg, R. Seager, P. A. O'Gorman, N. C. Johnson, On the future zonal contrasts of equatorial Pacific climate: Perspectives from observations, simulations, and theories. *Npj Clim. Atmospheric Sci.* **5**, 82 (2022).

9. R. Seager, M. Cane, N. Henderson, D.-E. Lee, R. Abernathey, H. Zhang, Strengthening tropical Pacific zonal sea surface temperature gradient consistent with rising greenhouse gases. *Nat. Clim. Change* **9**, 517–522 (2019).

10. U. K. Heede, A. V. Fedorov, Eastern equatorial Pacific warming delayed by aerosols and thermostat response to CO2 increase. *Nat. Clim. Change* **11**, 696–703 (2021).

11. Y.-T. Hwang, S.-P. Xie, P.-J. Chen, H.-Y. Tseng, C. Deser, Contribution of anthropogenic aerosols to persistent La Niña-like conditions in the early 21st century. *Proc. Natl. Acad. Sci.* **121**, e2315124121 (2024).

12. M. Watanabe, J.-L. Dufresne, Y. Kosaka, T. Mauritsen, H. Tatebe, Enhanced warming constrained by past trends in equatorial Pacific sea surface temperature gradient. *Nat. Clim. Change* **11**, 33–37 (2021).

13. M. Rugenstein, S. Dhame, D. Olonscheck, R. J. Wills, M. Watanabe, R. Seager, Connecting the SST Pattern Problem and the Hot Model Problem. *Geophys. Res. Lett.* **50**, e2023GL105488 (2023).

14. Y. Dong, K. C. Armour, D. S. Battisti, E. Blanchard-Wrigglesworth, Two-way teleconnections between the Southern Ocean and the tropical Pacific via a dynamic feedback. *J. Clim.* **35**, 6267–6282 (2022).

15. Y.-T. Hwang, S.-P. Xie, C. Deser, S. M. Kang, Connecting tropical climate change with Southern Ocean heat uptake. *Geophys. Res. Lett.* **44**, 9449–9457 (2017).

16. S. M. Kang, S.-P. Xie, Y. Shin, H. Kim, Y.-T. Hwang, M. F. Stuecker, B. Xiang, M. Hawcroft, Walker circulation response to extratropical radiative forcing. *Sci. Adv.* **6**, eabd3021 (2020).

17. H. Kim, S. M. Kang, J. E. Kay, S.-P. Xie, Subtropical clouds key to Southern Ocean teleconnections to the tropical Pacific. *Proc. Natl. Acad. Sci.* **119**, e2200514119 (2022).

18. S. M. Kang, Y. Yu, C. Deser, X. Zhang, I.-S. Kang, S.-S. Lee, K. B. Rodgers, P. Ceppi, Global impacts of recent Southern Ocean cooling. *Proc. Natl. Acad. Sci.* **120**, e2300881120 (2023).

19. S.-P. Xie, C. Deser, G. A. Vecchi, J. Ma, H. Teng, A. T. Wittenberg, Global Warming Pattern Formation: Sea Surface Temperature and Rainfall. *J. Clim.* **23**, 966–986 (2010).

20. M. T. Luongo, S.-P. Xie, I. Eisenman, S. Sun, Q. Peng, How the Subsurface Tropical Pacific Responds to Subtropical Surface Cooling: Implications for Cross-Equatorial Transport. *J. Clim.* **38**, 3313–3331 (2025).

21. Y. Dong, A. G. Pauling, S. Sadai, K. C. Armour, Antarctic ice-sheet meltwater reduces transient warming and climate sensitivity through the sea-surface temperature pattern effect. *Geophys. Res. Lett.* **49**, e2022GL101249 (2022).

22. D. L. Hartmann, The Antarctic ozone hole and the pattern effect on climate sensitivity. *Proc. Natl. Acad. Sci.* **119**, e2207889119 (2022).

23. Y. Dong, L. M. Polvani, Y.-T. Hwang, M. R. England, Stratospheric ozone depletion has contributed to the recent tropical La Niña-like cooling pattern. *Npj Clim. Atmospheric Sci.* **8**, 150 (2025).

24. B. Bronselaer, M. Winton, S. M. Griffies, W. J. Hurlin, K. B. Rodgers, O. V. Sergienko, R. J. Stouffer, J. L. Russell, Change in future climate due to Antarctic meltwater. *Nature* **564**, 53–58 (2018).

25. G. A. Schmidt, A. Romanou, L. Roach, K. Mankoff, Q. Li, C. D. Rye, M. Kelley, J. C. Marshall, J. J. M. Busecke, Anomalous meltwater from ice sheets and ice shelves is a historical forcing. *Geophys. Res. Lett.* **50**, e2023GL106530 (2023).

26. M. Sigmond, M. Reader, J. Fyfe, N. Gillett, Drivers of past and future Southern Ocean change: Stratospheric ozone versus greenhouse gas impacts. *Geophys. Res. Lett.* **38** (2011).

27. D. Ferreira, J. Marshall, C. M. Bitz, S. Solomon, A. Plumb, Antarctic Ocean and sea ice response to ozone depletion: A two-time-scale problem. *J. Clim.* **28**, 1206–1226 (2015).

28. S. M. Kang, P. Ceppi, Y. Yu, I.-S. Kang, Recent global climate feedback controlled by Southern Ocean cooling. *Nat. Geosci.* **16**, 775–780 (2023).

29. S. M. Kang, M. Hawcroft, B. Xiang, Y.-T. Hwang, G. Cazes, F. Codron, T. Crueger, C. Deser, Ø. Hodnebrog, H. Kim, others, Extratropical–tropical interaction model intercomparison project (ETIN-MIP): Protocol and initial results. *Bull. Am. Meteorol. Soc.* **100**, 2589–2606 (2019).

30. X. Zhang, C. Deser, L. Sun, Is there a tropical response to recent observed Southern Ocean cooling? *Geophys. Res. Lett.* **48**, e2020GL091235 (2021).

31. Y. Zheng, M. Rugenstein, M. J. Alessi, The relationship between the Southern Ocean and the southeastern subtropical Pacific in unforced and forced climate model simulations. *J. Clim.* (2025).

32. R. Seager, M. Hoerling, Atmosphere and ocean origins of North American droughts. *J. Clim.* **27**, 4581–4606 (2014).

33. H. Kim, S. M. Kang, A. G. Pendergrass, F. Lehner, Y. Shin, P. Ceppi, S.-W. Yeh, S.-Y. Song, Higher precipitation in East Asia and western United States expected with future Southern Ocean warming. *Nat. Geosci.*, 1–9 (2025).

34. Y. Kosaka, S.-P. Xie, Recent global-warming hiatus tied to equatorial Pacific surface cooling. *Nature* **501**, 403–407 (2013).

35. O. Adam, T. Bischoff, T. Schneider, Seasonal and interannual variations of the energy flux equator and ITCZ. Part I: Zonally averaged ITCZ position. *J. Clim.* **29**, 3219–3230 (2016).

36. B. Tian, X. Dong, The double-ITCZ bias in CMIP3, CMIP5, and CMIP6 models based on annual mean precipitation. *Geophys. Res. Lett.* **47**, e2020GL087232 (2020).

37. J.-Y. Zhuo, C.-Y. Lee, A. Sobel, R. Seager, S. J. Camargo, Y.-H. Lin, B. Fosu, K. A. Reed, A More La Niña–Like Response to Radiative Forcing after Flux Adjustment in CESM2. *J. Clim.* **38**, 1037–1050 (2025).

38. P. Breul, P. Ceppi, P. Nowack, The importance of stratocumulus clouds for projected warming patterns and circulation changes. *EGUsphere* **2025**, 1–22 (2025).

39. W.-T. Hsiao, Y.-T. Hwang, Y.-J. Chen, S. M. Kang, The role of clouds in shaping tropical Pacific response pattern to extratropical thermal forcing. *Geophys. Res. Lett.* **49**, e2022GL098023 (2022).

40. A. G. Pauling, C. M. Bitz, I. J. Smith, P. J. Langhorne, The response of the Southern Ocean and Antarctic sea ice to freshwater from ice shelves in an Earth system model. *J. Clim.* **29**, 1655–1672 (2016).

41. A. Purich, M. H. England, W. Cai, A. Sullivan, P. J. Durack, Impacts of broad-scale surface freshening of the Southern Ocean in a coupled climate model. *J. Clim.* **31**, 2613–2632 (2018).

42. C. D. Rye, J. Marshall, M. Kelley, G. Russell, L. S. Nazarenko, Y. Kostov, G. A. Schmidt, J. Hansen, Antarctic glacial melt as a driver of recent Southern Ocean climate trends. *Geophys. Res. Lett.* **47**, e2019GL086892 (2020).

641 43. N. Swart, T. Martin, R. Beadling, J.-J. Chen, M. H. England, R. Farneti, S. M. Griffies, T. Hatterman, F. A.
642 Haumann, Q. Li, others, The Southern Ocean Freshwater release model experiments Initiative (SOFIA):
643 Scientific objectives and experimental design. *EGUsphere* **2023**, 1–30 (2023).

644 44. X. Xu, T. Martin, R. L. Beadling, J. Liu, S. Bischof, T. Hattermann, W. Huo, Q. Li, J. C. Marshall, M. Muilwijk,
645 others, Robustness and mechanisms of the atmospheric response over the Southern Ocean to idealized
646 freshwater input around Antarctica. *Geophys. Res. Lett.* **52**, e2024GL113734 (2025).

647 45. L. A. Roach, K. D. Mankoff, A. Romanou, E. Blanchard-Wrigglesworth, T. W. Haine, G. A. Schmidt, Winds
648 and meltwater together lead to Southern Ocean surface cooling and sea ice expansion. *Geophys. Res. Lett.* **50**,
649 e2023GL105948 (2023).

650 46. R. Garreaud, D. S. Battisti, Interannual (ENSO) and interdecadal (ENSO-like) variability in the Southern
651 Hemisphere tropospheric circulation. *J. Clim.* **12**, 2113–2123 (1999).

652 47. M. A. Alexander, I. Bladé, M. Newman, J. R. Lanzante, N.-C. Lau, J. D. Scott, The atmospheric bridge: The
653 influence of ENSO teleconnections on air–sea interaction over the global oceans. *J. Clim.* **15**, 2205–2231 (2002).

654 48. J. M. Kang, T. A. Shaw, S. M. Kang, I. R. Simpson, Y. Yu, Revisiting the reanalysis-model discrepancy in
655 Southern Hemisphere winter storm track trends. *Npj Clim. Atmospheric Sci.* **7**, 252 (2024).

656 49. L. Wang, K. M. Grise, Tropical Pacific Sea Surface Temperature Gradient Biases Shape Present-Day and Future
657 Precipitation Projections Over Southern Hemisphere Midlatitudes. *Geophys. Res. Lett.* **53**, e2025GL120299
658 (2026).

659 50. Q. Wu, M. Yejian, A. Hu, N. Rosenbloom, L. Zhang, H. Liu, s Liu, L. Yang, C. Yang, Pacific sub-decadal sea
660 surface temperature variations contributed to recent Antarctic Sea ice decline trend. *Nat. Commun.* **16** (2025).

661 51. S. G. Yeager, P. Chang, G. Danabasoglu, N. Rosenbloom, Q. Zhang, F. S. Castruccio, A. Gopal, M. Cameron
662 Rencurrel, I. R. Simpson, Reduced Southern Ocean warming enhances global skill and signal-to-noise in an
663 eddy-resolving decadal prediction system. *Npj Clim. Atmospheric Sci.* **6**, 107 (2023).

664 52. C. Li, J.-S. von Storch, J. Marotzke, Deep-ocean heat uptake and equilibrium climate response. *Clim. Dyn.* **40**,
665 1071–1086 (2013).

666 53. K. C. Armour, J. Marshall, J. R. Scott, A. Donohoe, E. R. Newsom, Southern Ocean warming delayed by
667 circumpolar upwelling and equatorward transport. *Nat. Geosci.* **9**, 549–554 (2016).

668 54. W. Cai, L. Gao, Y. Luo, X. Li, X. Zheng, X. Zhang, X. Cheng, F. Jia, A. Purich, A. Santoso, others, Southern
669 Ocean warming and its climatic impacts. *Sci. Bull.* **68**, 946–960 (2023).

670 55. C. Eayrs, X. Li, M. N. Raphael, D. M. Holland, Rapid decline in Antarctic sea ice in recent years hints at future
671 change. *Nat. Geosci.* **14**, 460–464 (2021).

672 56. A. Purich, E. W. Doddridge, Record low Antarctic sea ice coverage indicates a new sea ice state. *Commun.
673 Earth Environ.* **4**, 314 (2023).

674 57. T. Fan, C. Deser, D. P. Schneider, Recent Antarctic sea ice trends in the context of Southern Ocean surface
675 climate variations since 1950. *Geophys. Res. Lett.* **41**, 2419–2426 (2014).

676 58. M. England, L. Polvani, L. Sun, Robust Arctic warming caused by projected Antarctic sea ice loss. *Environ. Res.
677 Lett.* **15**, 104005 (2020).

678 59. S. A. Klein, A. Hall, J. R. Norris, R. Pincus, Low-Cloud Feedbacks from Cloud-Controlling Factors: A Review.
679 *Surv. Geophys.* **38**, 1307–1329 (2017).

680 60. R. F. Adler, G. J. Huffman, A. Chang, R. Ferraro, P.-P. Xie, J. Janowiak, B. Rudolf, U. Schneider, S. Curtis, D.
681 Bolvin, others, The version-2 global precipitation climatology project (GPCP) monthly precipitation analysis
682 (1979–present). *J. Hydrometeorol.* **4**, 1147–1167 (2003).

61. H. Hersbach, B. Bell, P. Berrisford, S. Hirahara, A. Horányi, J. Muñoz-Sabater, J. Nicolas, C. Peubey, R. Radu, D. Schepers, others, The ERA5 global reanalysis. *Q. J. R. Meteorol. Soc.* **146**, 1999–2049 (2020).

62. N. J. Lenssen, G. A. Schmidt, J. E. Hansen, M. J. Menne, A. Persin, R. Ruedy, D. Zyss, Improvements in the GISTEMP uncertainty model. *J. Geophys. Res. Atmospheres* **124**, 6307–6326 (2019).

63. T. Slater, I. R. Lawrence, I. N. Otosaka, A. Shepherd, N. Gourmelen, L. Jakob, P. Tepes, L. Gilbert, P. Nienow, Earth's ice imbalance. *The Cryosphere* **15**, 233–246 (2021).

Acknowledgments

We thank Hanjun Kim for sharing cloud feedback data for ETIN-MIP models and Robert Jnglin Wills for helpful discussions. We thank the editor and four anonymous reviewers for their constructive feedback. The authors would like to acknowledge high-performance computing support from the Derecho system (doi:10.5065/qx9a-pg09) provided by the NSF National Center for Atmospheric Research (NCAR), sponsored by the National Science Foundation.

Funding:

Y.D. was supported by a grant from the W. M. Keck Foundation. Y.-T. Hwang and R.-J. Hu were supported by the Ministry of Science and Technology Council (NSTC), Taiwan, under Grant NSTC112-2111-M-002-016-MY4. L.R. was supported by the Initiative and Networking Fund of the Helmholtz Association (no. VH-NG-20-10)

Author contributions: YD designed and led the research; KL performed the ``cloud-adjusted'' CESM1 simulations using the code developed by PB and PC. RJH and YTH performed the CMIP6 mean-state ITCZ and cloud feedback analysis. LR contributed the GISS-E2-1-G meltwater simulations. All co-authors contributed to the original and final drafts.

Competing interests: The authors declare no competing interests.

Data and materials availability: Output from the idealized CESM1 simulations will be available on Zenodo upon publication. CMIP6 data were obtained via ESGF at https://aims2.llnl.gov/search/cmip6/. ALl observational data are publicly available. GPCP precipitation, ERSSTv5 SST and COBE SST data were obtained from NOAA PSL at https://psl.noaa.gov/data/gridded/data.gpcp.html, https://psl.noaa.gov/data/gridded/data.noaa.ersst.v5.html and https://psl.noaa.gov/data/gridded/data.cobe.html. ERA5 reanalysis was obtained from the Copernicus Climate Data Store at https://cds.climate.copernicus.eu/datasets/reanalysis-era5-single-levels-monthly-means. GISTEMPv4 SST data were obtained from NASA GISS at https://data.giss.nasa.gov/gistemp/. ETIN-MIP simulation output is available at https://zenodo.org/records/3362615. SOFIA meltwater simulation output is available at https://sofiamip.github.io/data-access.html. GISS-E2-1-G control and meltwater simulation output was obtained from the NCCS portal at https://portal.nccs.nasa.gov/datashare/giss_cmip6/CMIP/NASA-GISS/GISS-E2-1-G/ and is also available through ESGF.

Science Advances
AAAS

Supplementary Materials for

Tropical impacts of the Southern Ocean underestimated by mean-state biases

Yue Dong *et al.*

*Corresponding author. Email: ydong@atmos.ucla.edu

This PDF file includes:

Figs. S1 to S8

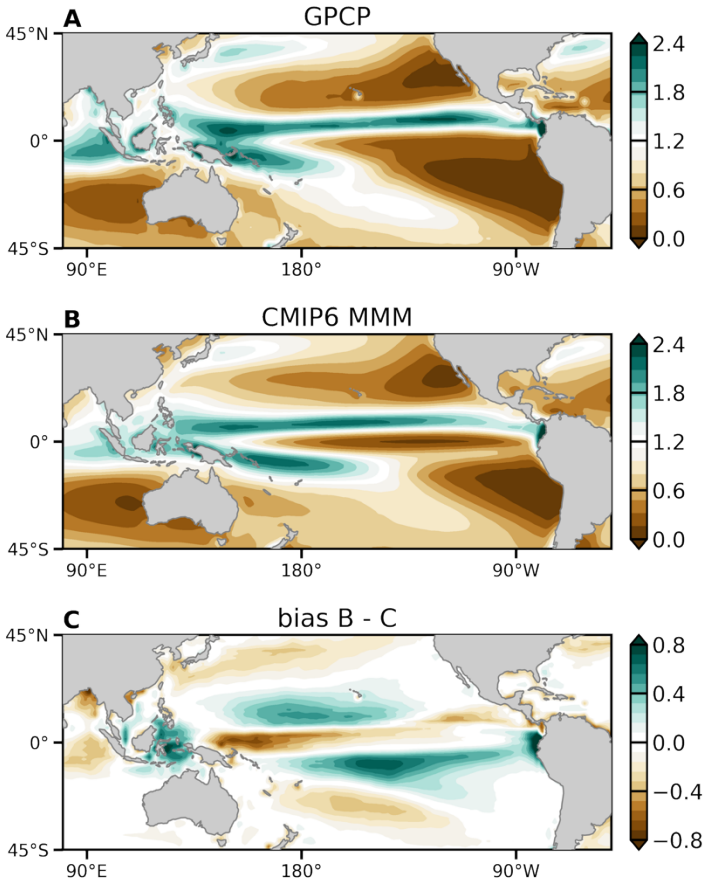

Fig. S1.

Annual-mean precipitation climatology (1979-2024) in observations and CMIP6 models. (A) GPCP observations; (B) CMIP6 historical multi-model mean; (C) differences between observation and CMIP6 multi-model mean. Precipitation patterns have been normalized by the tropical mean (15°S–15°N).

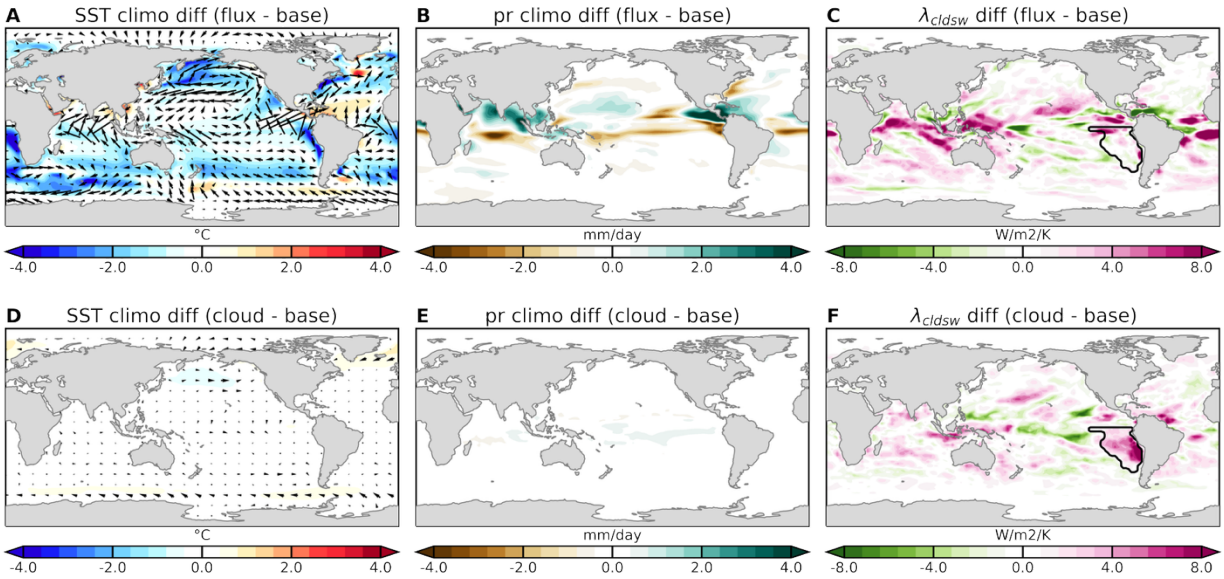

Fig. S2.

Differences in mean states between "adjusted" and "base" simulations within CESM1. Top row: difference between "flux-adjusted" run and the "base" run; bottom row: difference between "cloud-adjusted" and the "base" run. From left to right are SST (K), precipitation (mm/day), and shortwave cloud feedback ($Wm^{-2}K^{-1}$). Black contours in (C) and (F) illustrate the subtropical Pacific stratocumulus deck region where cloud adjustment is applied.

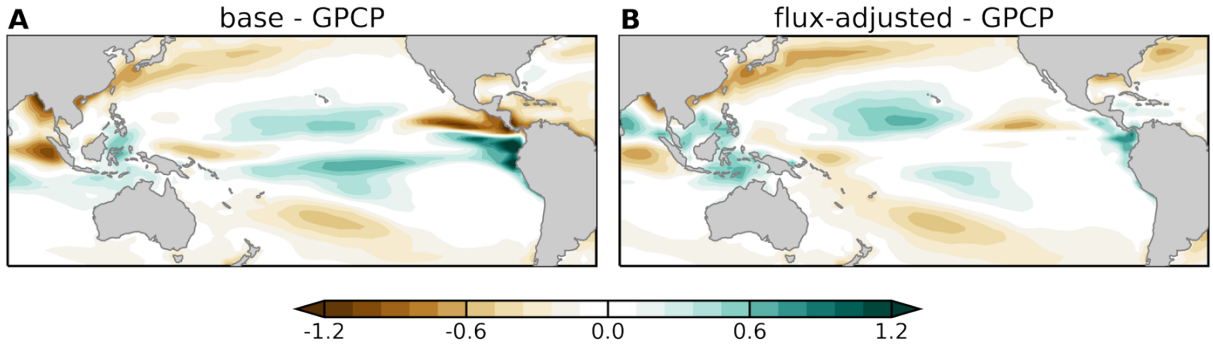

Fig. S3.

Annual-mean precipitation climatology between GPCP observations and CESM1 simulations. (A) CESM1 "base" control run minus GPCP. (B) CESM1 "flux-adjusted" control run minus GPCP. Same with Fig. S1, all precipitation mean states have been normalized by the tropical mean (15°S–15°N).

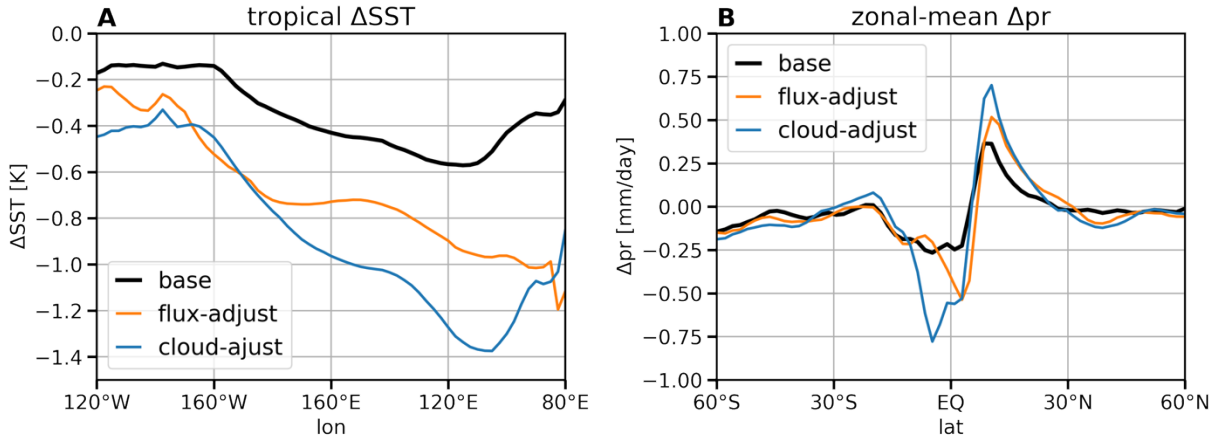

Fig. S4.

Tropical SST and zonal-mean precipitation response to SO qflux forcing simulated in CESM1 simulations. (A) Tropical Pacific SST averaged over 10°S–10°N. (B) Zonal-mean precipitation between 60°S–60°N.

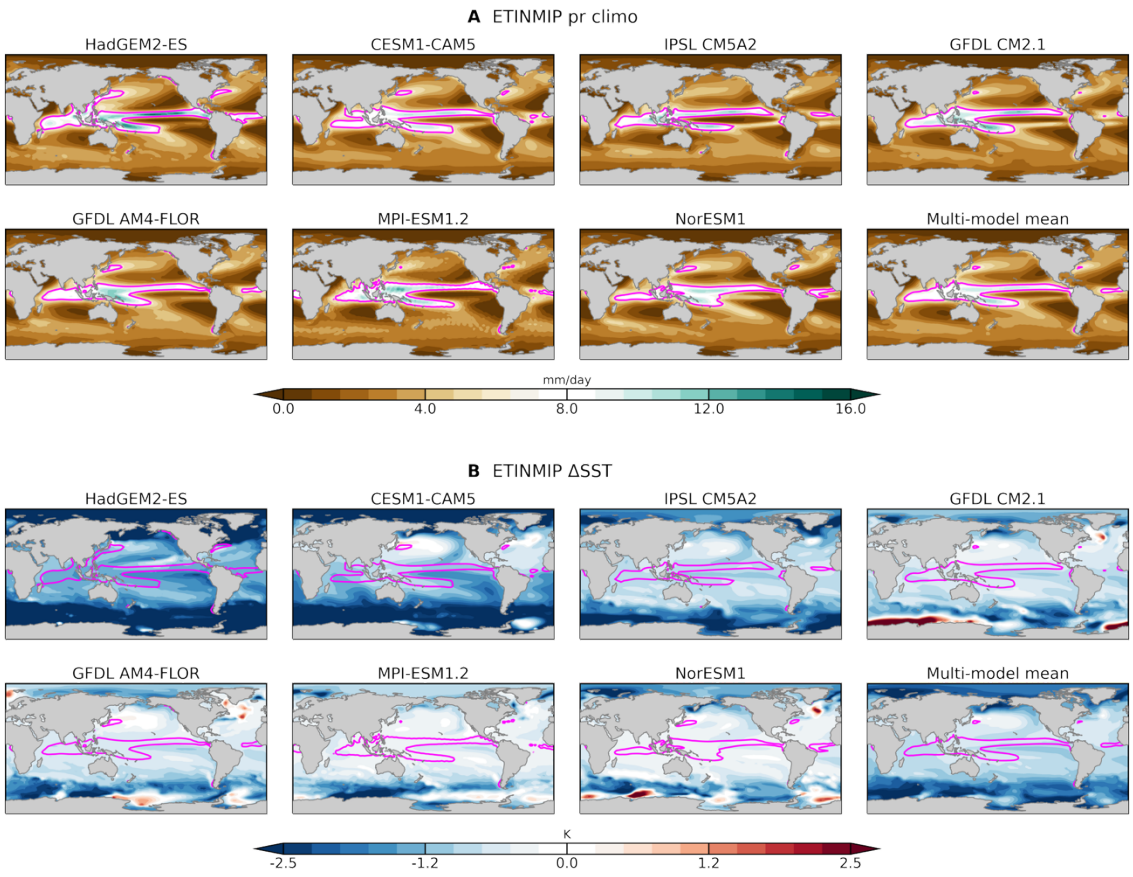

Fig. S5.

Individual ETIN-MIP model result. (A) mean-state precipitation from the ETINMIP control simulations; (B) SST response to imposed SH extratropical radiative forcing from the ETINMIP *stoa* simulations. Magenta contours show the 6 mm/day contour of precipitation climatology. The bottom right panels in both (A) and (B) show the multi-model mean results.

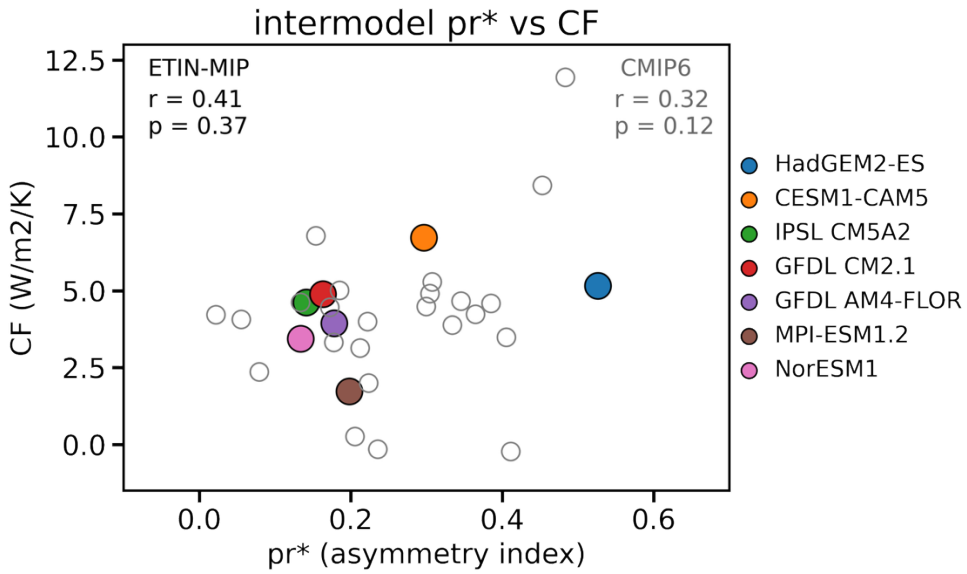

Fig. S6.

Inter-model correlation between mean-state precipitation index (*pr**) and subtropical eastern Pacific cloud-SST feedback (CF). Colored scatters represent 7 ETIN-MIP models; grey unfilled scatters represent 24 CMIP6 GCMs. Correlation coefficient (*r*) and p-values (*p*) for ETIN-MIP and CMIP6 inter-model correlations are shown in the top left and top right corners, respectively. Both *pr** and CF values are computed from model piControl simulations.

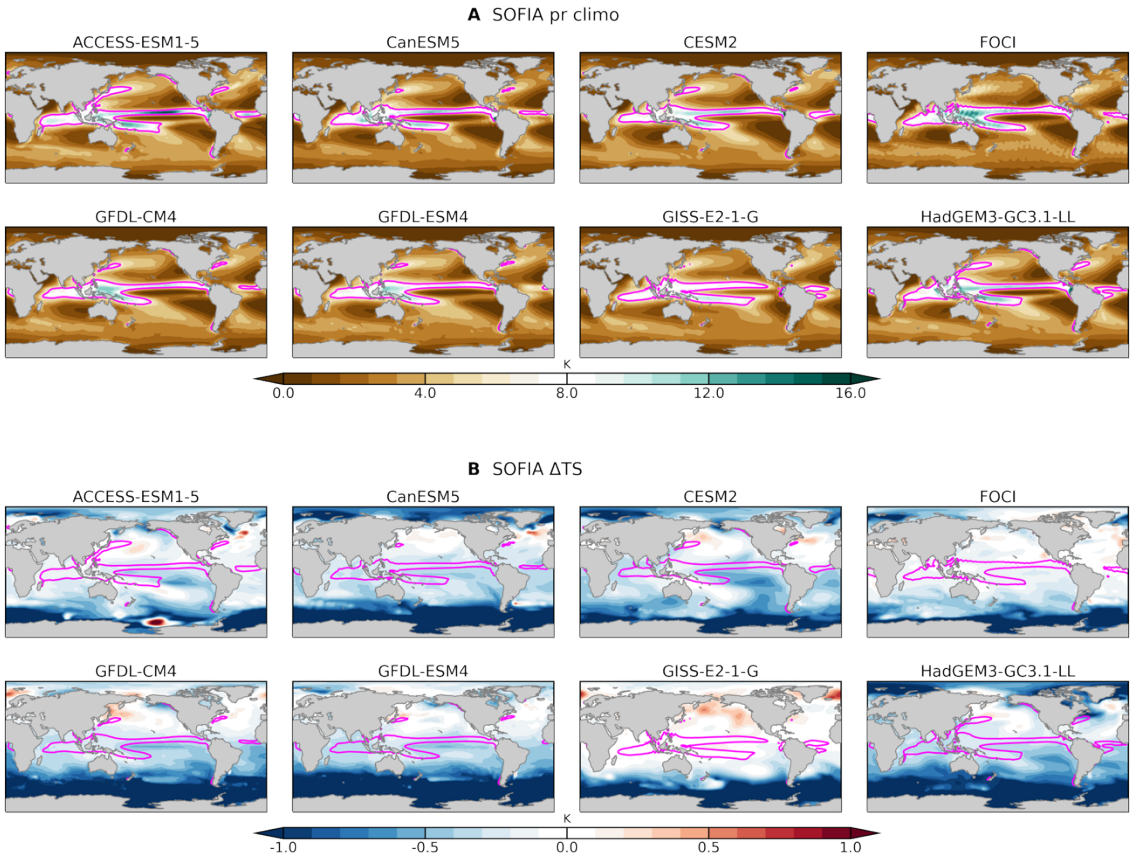

Fig. S7.

Individual SOFIA model results. (A) mean-state precipitation from the SOFIA control simulations; (B) surface air temperature response to imposed Antarctic meltwater from SOFIA hosing simulations. Magenta contours show the 6 mm/day contour of precipitation climatology.

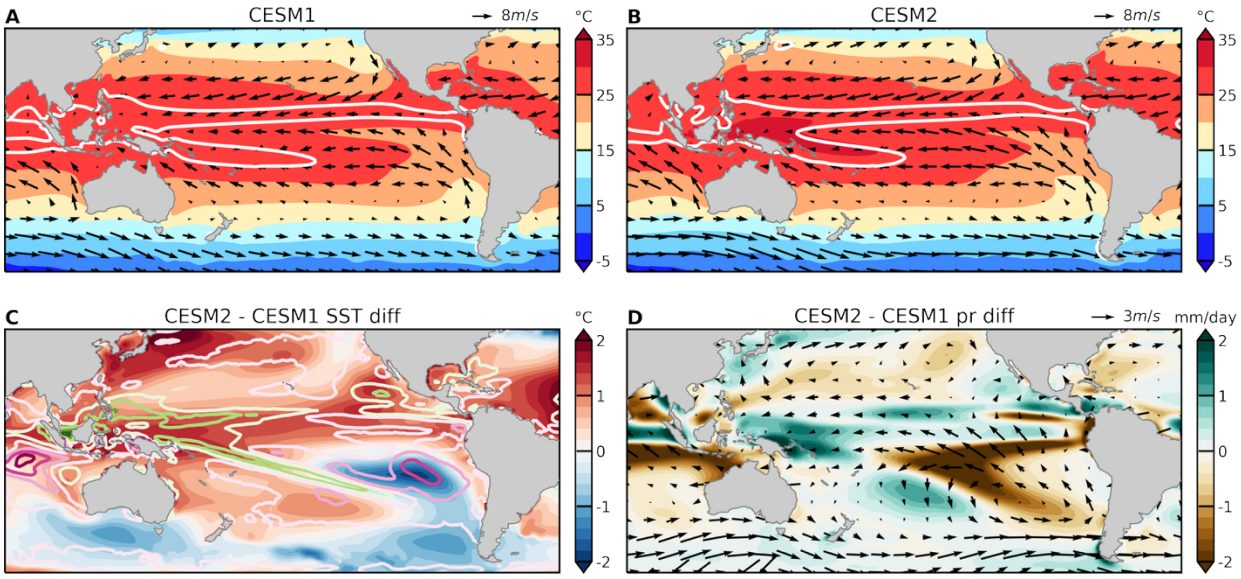

Fig. S8.

CESM1 and CESM2 mean-state climates from piControl simulations. (A-B) mean-state SST (shading), surface winds (arrows) and precipitation (6 mm/day contour) in CESM1 and CESM2. (C) Difference in SST (shading) and cloud-SST feedback (contours) between CESM1 and CESM2. Pink (green) denotes more positive (negative) cloud-SST feedback values. (D) Differences in precipitation (shading) and surface winds (arrows).